INORGANIC CHEMISTRY
FRONTIERS

RESEARCH ARTICLE

View Article Online
View Journal | View Issue

Check for updates

Cite this: *Inorg. Chem. Front.*, 2025, **12**, 2266

Luminescent iridium(III) 2-cyanobenzothiazole complexes as site-specific labels to afford peptide-based phosphorogenic probes and hydrogels for enzyme activity sensing, cancer imaging and photodynamic therapy†

Jun-Wen Xu, [a] Lawrence Cho-Cheung Lee, [a] Alex Man-Hei Yip, [a,b] Guang-Xi Xu, [a] Peter Kam-Keung Leung [a,c] and Kenneth Kam-Wing Lo *[a,c]

Site-specific modification of biomolecules is crucial to the development of functional constructs for biomedical applications, offering precise control over the number and location of the functional handles incorporated. In this work, we designed, synthesised and characterised three luminescent cyclometallated iridium(III) complexes bearing a 2-cyanobenzothiazole (CBT) moiety $[Ir(N^C)_2(bpy\text{-}CBT)](PF_6)$ (HN^C = 2-(2,4-difluorophenyl)pyridine (Hdfppy) (**1**), 2-phenylpyridine (Hppy) (**2**), methyl 2-phenyl-4-quinolinecarboxylate (Hpqe) (**3**); bpy-CBT = 4-(2-cyanobenzo[*d*]thiazol-6-yl)oxymethyl-4′-methyl-2,2′-bipyridine) as site-specific labels for N-terminal cysteine (NCys). These complexes displayed high reactivity and selectivity towards NCys, enabling facile peptide conjugation *via* the CBT–NCys condensation reaction. Complex **2** was used to prepare a peptide-based phosphorogenic probe **2-MMP-QSY7** for matrix metalloproteinase-2/9 (MMP-2/9) activity sensing and photocytotoxic applications. The conjugate showed substantial emission enhancement (I/I_o = 9.8) in the presence of MMP-2/9, which allowed for the sensitive detection of MMP-2/9 activity in live cells and the facile differentiation of cancer and normal cells. The conjugate also exhibited controllable singlet oxygen generation and thereby photocytotoxicity in these cell lines. Additionally, complex **2** was utilised to fabricate two types of hydrogels: a non-biodegradable hydrogel **Gel-1** as a cell culture scaffold integrated with MMP-2/9 sensing capability for examining the enzyme activity in 3D cell culture; and a biodegradable hydrogel **Gel-2** as an MMP-2/9-sensitive carrier for selective delivery of luminescent iridium(III) complexes into cancer cells for imaging and photocytotoxic applications. The results of this work will contribute to the development of site-specific bioconjugation reagents with interesting photophysical properties, facilitating the construction of photofunctional peptide conjugates and biomaterials for biosensing, bioimaging, phototherapy and drug delivery applications.

Received 20th December 2024,
Accepted 19th January 2025

DOI: 10.1039/d4qi03276d

rsc.li/frontiers-inorganic

Open Access Article. Published on 28 de gener 2025. Downloaded on 13/2/2026 2:23:50.
This article is licensed under a Creative Commons Attribution-NonCommercial 3.0 Unported Licence.

10th anniversary statement

As a scientist working at the interface of inorganic chemistry and biology, I am pleased to contribute to the 10th-anniversary collection for *Inorganic Chemistry Frontiers*. Since the journal was established in 2014, my group has published two Review Articles on developments in transition metal complexes used as cellular probes, intracellular sensors, bioimaging reagents and (photo)therapeutic agents. Over the past 10 years, I have observed this journal provide a platform for innovative research and reviews, fostering new ideas and collaborations within our community. Congratulations to *Inorganic Chemistry Frontiers* on this milestone. I look forward to seeing the journal continue to support research in inorganic chemistry.

[a]*Department of Chemistry, City University of Hong Kong, Tat Chee Avenue, Kowloon, Hong Kong, P. R. China. E-mail: bhkenlo@cityu.edu.hk*
[b]*Laboratory for Synthetic Chemistry and Chemical Biology Limited, Units 1503–1511, 15/F, Building 17 W, Hong Kong Science Park, New Territories, Hong Kong, P. R. China*
[c]*State Key Laboratory of Terahertz and Millimetre Waves, City University of Hong Kong, Tat Chee Avenue, Kowloon, Hong Kong, P. R. China*

† Electronic supplementary information (ESI) available. See DOI: https://doi.org/10.1039/d4qi03276d

This journal is © the Partner Organisations 2025

Open Access Article. Published on 28 de gener 2025. Downloaded on 13/2/2026 2:23:50.
This article is licensed under a Creative Commons Attribution-NonCommercial 3.0 Unported Licence.

Introduction

Bioconjugation reactions that enable site-specific modification of peptides and proteins are important to the interrogation of the functions of these biomolecules and their associated biological processes as well as to the development of novel conjugates for biomedical applications.[1,2] Among the various strategies developed, the modification of N-terminal cysteine (NCys) is a highly attractive approach due to the relatively low natural abundance of cysteine (Cys) in natural peptides and proteins, and the distinctive reactivity of its 1,2-aminothiol group that allows for site-specific labelling while retaining the modifiability of other side chains, including the internal and C-terminal Cys residues.[3–5] Several reagents have been developed for NCys modification, including thioesters,[6] 2-cyanobenzothiazole (CBT),[7] 2-formylphenylboronic acid (FPBA),[8–10] 2-((alkylthio)(aryl)methylene)malononitrile (TAMM)[11] and cyclopropenone (CPO).[12] In particular, the firefly luciferin-inspired click reaction between CBT and NCys has gained significant attention due to its high efficiency, selectivity and biocompatibility, and this reaction has been widely applied in protein labelling, molecular imaging and nanomaterial fabrication.[13–15]

There has been increasing interest in photofunctional transition metal–peptide conjugates for imaging and therapeutic applications.[16–18] This interest stems from the intriguing photophysical properties of transition metal complexes, including intense and long-lived emission, efficient reactive oxygen species (ROS) photosensitisation and high photostability. Peptide conjugation can endow these photoactive complexes with interesting biological behaviour such as receptor targeting,[19–22] cell penetrating,[23–25] organelle targeting,[26–29] enzyme-responsiveness[30] and self-assembly capabilities.[31] Our group has exploited various chemoselective reactions in the development of metal–peptide conjugates for organelle staining, enzyme sensing, cancer imaging and photocytotoxic applications.[32–37] We anticipate that the incorporation of a CBT moiety into iridium(III) complexes will lead to new site-specific labels for the construction of peptide-based reagents and biomaterials for biomedical applications.

Herein, we report the design, synthesis and characterisation of three luminescent cyclometallated iridium(III) polypyridine complexes bearing a CBT moiety $[Ir(N^C)_2(bpy\text{-}CBT)](PF_6)$ (HN^C = 2-(2,4-difluorophenyl)pyridine (Hdfppy) (**1**), 2-phenylpyridine (Hppy) (**2**), methyl 2-phenyl-4-quinolinecarboxylate (Hpqe) (**3**); bpy-CBT = 4-(2-cyanobenzo[*d*]thiazol-6-yl)oxymethyl-4′-methyl-2,2′-bipyridine) (Scheme 1). These complexes displayed high reactivity and selectivity towards NCys, enabling facile peptide conjugation *via* the CBT–NCys condensation reaction. Complex **2** was employed to prepare a peptide-based phosphorogenic probe for enzyme sensing and controllable photocytotoxic applications (Fig. 1a). This complex was also used to fabricate two types of enzyme-responsive hydrogels for the *in situ* detection of enzyme activity in 3D cell culture models (Fig. 1b), as well as for cancer-specific imaging and photocytotoxic applications (Fig. 1c).

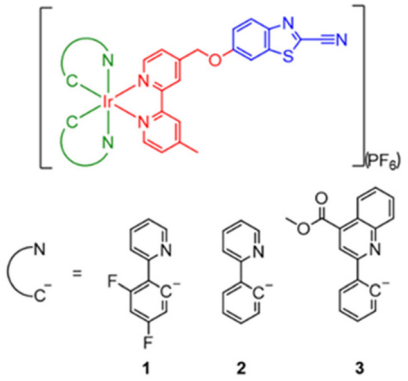

Scheme 1 Structures of complexes **1–3**.

Results and discussion

Synthesis and characterisation

The synthesis of the diimine ligand bpy-CBT involved the reaction of 6-hydroxybenzo[*d*]thiazole-2-carbonitrile with 4-bromomethyl-4′-methyl-2,2′-bipyridine (bpy-Br). The iridium(III) complexes **1–3** were prepared from the reaction of respective iridium(III) dimers $[Ir_2(N^C)_4Cl_2]$ with bpy-CBT in CH_2Cl_2/CH_3OH, followed by anion exchange with KPF_6, purification by column chromatography and recrystallisation from CH_2Cl_2/Et_2O. All the complexes were characterised by high-resolution ESI-MS, ^1H and ^{13}C NMR and IR spectroscopy. Detailed synthetic procedures and characterisation data are included in the ESI.†

Photophysical properties

Complexes **1–3** displayed intense spin-allowed intraligand (^1IL) ($\pi \rightarrow \pi^*$) (bpy-CBT and N^C) absorption features in the UV region (*ca.* 252–352 nm, ε on the order of 10^4 dm^3 mol^{-1} cm^{-1}) and weaker spin-allowed metal-to-ligand charge transfer (^1MLCT) ($d\pi(Ir) \rightarrow \pi^*$(bpy-CBT and N^C)) absorption shoulders or bands in a lower energy region (*ca.* 378–440 nm) (Table S1 and Fig. S1, ESI†).[38–40] The weaker absorption tailing beyond 467 nm is assigned to spin-forbidden ^3MLCT ($d\pi(Ir) \rightarrow \pi^*$(bpy-CBT and N^C)) transitions. Upon irradiation, all the complexes exhibited intense and long-lived green to red emission in fluid solutions under ambient conditions and in low-temperature alcohol glass (Table 1 and Fig. S2, ESI†). The complexes showed broad and featureless emission bands with positive solvatochromism in fluid solutions at 298 K and their emission maxima displayed significant blue shifts upon cooling the samples to 77 K, suggestive of a predominant ^3MLCT ($d\pi(Ir) \rightarrow \pi^*$(bpy-CBT and N^C))/triplet ligand-to-ligand charge transfer (^3LLCT) ($\pi(N^C) \rightarrow \pi^*$(bpy-CBT)) emissive state.[38–40] Additionally, all the complexes exhibited high singlet oxygen ($^1O_2$) generation efficiencies in aerated CH_3CN (Φ_Δ = 0.59–0.85) (Table S2, ESI†).

Reactivity and selectivity towards NCys

We first studied the reaction of complexes **1–3** with NCys by using L-Cys as a model (Fig. 2a). The complexes (100 μM) were

Open Access Article. Published on 28 de gener 2025. Downloaded on 13/2/2026 2:23:50.
This article is licensed under a Creative Commons Attribution-NonCommercial 3.0 Unported Licence.

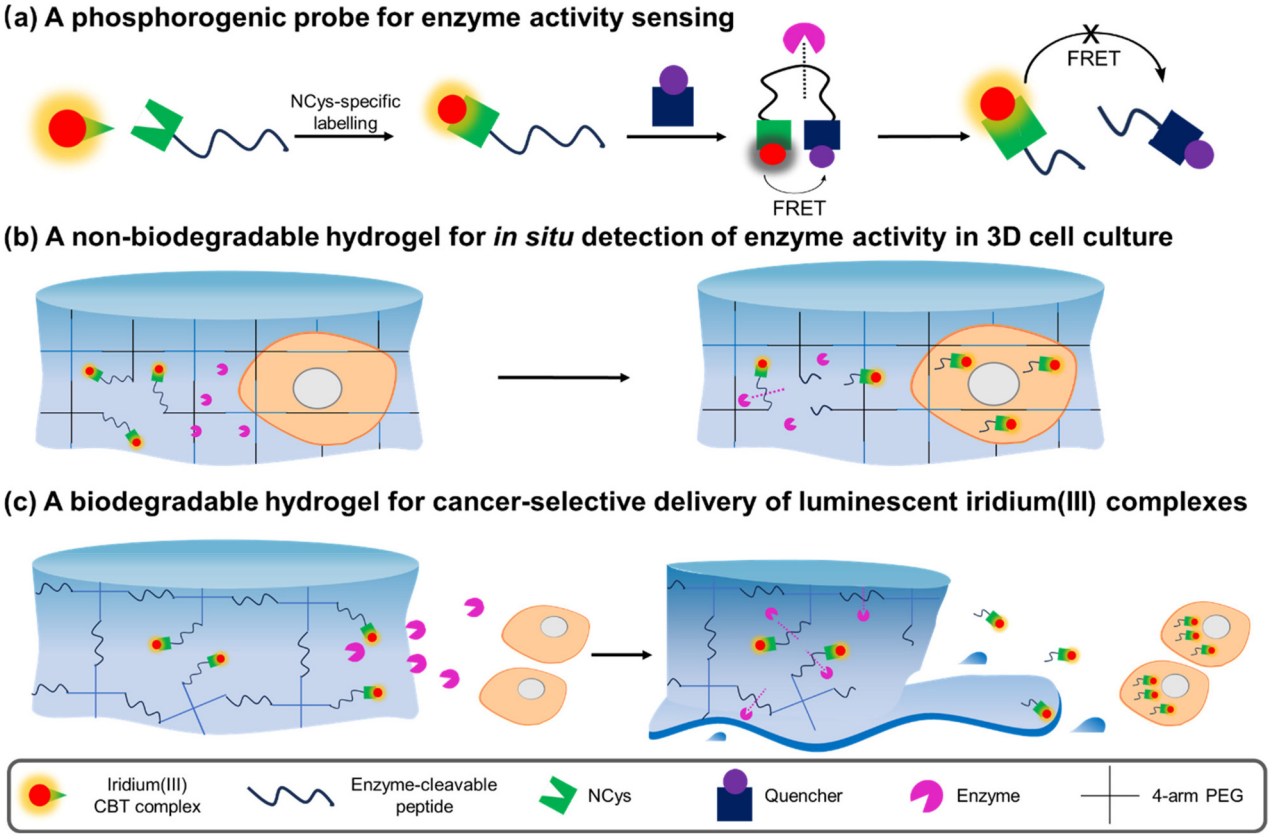

Fig. 1 Schematic illustration of the utilisation of iridium(III) CBT complexes in the construction of (a) a FRET-based phosphorogenic probe for enzyme activity sensing; (b) a non-biodegradable hydrogel for *in situ* detection of enzyme activity in 3D cell culture; and (c) a biodegradable hydrogel for cancer-selective delivery of luminescent iridium(III) complexes.

Table 1 Photophysical data of complexes **1–3** at 298 K

Complex	Medium (T/K)	λ_{em}[a]/nm	τ_o[b]/μs	Φ_{em}[c]
1	CH_2Cl_2 (298)	523	4.04	0.90
	CH_3CN (298)	526	3.40	0.46
	Glass[d] (77)	450 (max), 483, 516 sh	4.06	
2	CH_2Cl_2 (298)	584	0.18	0.13
	CH_3CN (298)	589	0.10	0.04
	Glass[d] (77)	510, 527 sh	4.00	
3	CH_2Cl_2 (298)	621	0.46	0.09
	CH_3CN (298)	638	0.20	0.03
	Glass[d] (77)	598, 645 sh	4.87	

[a] λ_{ex} = 350 nm. [b] The lifetimes were measured at the emission maxima (λ_{ex} = 355 nm). [c] The emission quantum yields were determined using $[Ru(bpy)_3]Cl_2$ (Φ_{em} = 0.04 in aerated H_2O, λ_{ex} = 455 nm) as a reference. [d] EtOH/CH_3OH (4 : 1, v/v).

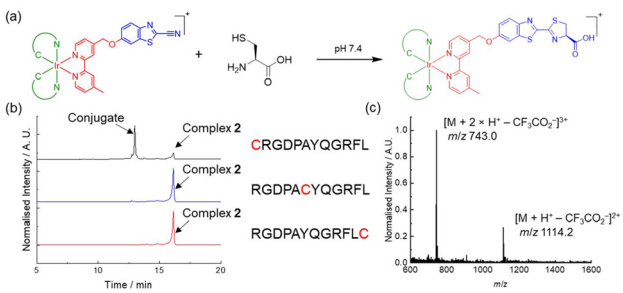

Fig. 2 (a) Reaction of L-Cys with iridium(III) CBT complexes **1–3**. (b) HPLC chromatograms (λ_{abs} = 350 nm) of the reaction mixtures of complex **2** (150 μM), peptide (150 μM), and TCEP (100 μM) in PBS/CH_3CN (9 : 1, v/v) at 298 K for 4 h. Peptide: CRGDPAYQGRFL (black), RGDPACYQGRFL (blue) and RGDPAYQGRFLC (red). (c) ESI mass spectrum of the eluent collected at t_R = 13.0 min of the reaction of complex **2** and CRGDPAYQGRFL.

incubated with L-Cys (250 μM) in phosphate-buffered saline (PBS)/CH_3CN (9 : 1, v/v) containing tris(2-carboxyethyl)phosphine (TCEP) (100 μM) at 37 °C. Reversed-phase high-performance liquid chromatography (RP-HPLC) results indicated that all the complexes were converted to their corresponding products **1-Cys–3-Cys** within 4 h (Fig. S3, ESI†). The formation of the iridium(III)–Cys conjugates was confirmed by ESI-MS (Fig. S4, ESI†). Complex **2** was selected as an example for further studies due to its better solubility in aqueous solutions. To examine its chemoselectivity, the complex was incubated with various biologically relevant nucleophiles, including glutathione, histidine, lysine, serine and threonine. As revealed by ESI-MS analysis, no reactions were detected and the complex remained intact (Fig. S5, ESI†). Furthermore, we

 This journal is © the Partner Organisations 2025

Open Access Article. Published on 28 de gener 2025. Downloaded on 13/2/2026 2:23:50.
This article is licensed under a Creative Commons Attribution-NonCommercial 3.0 Unported Licence.

utilised a breast cancer cell-targeting peptide RGDPAYQGRFL[41] as a model and modified it with a Cys residue at the N-terminus (CRGDPAYQGRFL), middle (RGDPACYQGRFL) and C-terminus (RGDPAYQGRFLC) to investigate the regioselectivity of the complex. A new peak (t_R = 13.0 min) was observed in the HPLC chromatogram only upon incubation of complex **2** with the NCys-containing peptide CRGDPAYQGRFL (Fig. 2b). The formation of the peptide conjugate was further verified by ESI-MS (Fig. 2c). These results indicate that the CBT complexes displayed high reactivity as well as excellent chemo- and regioselectivity towards NCys.

Preparation of phosphorogenic probes for MMP-2/9 sensing

Given the high reactivity as well as excellent chemo- and regioselectivity of the CBT complexes towards NCys, we explored the application of these complexes in the construction of peptide-based phosphorogenic probes for sensing enzyme activity. Matrix metalloproteinases (MMPs) are a group of zinc-dependent endopeptidases present in the extracellular matrix (ECM), which are responsible for the regulation of ECM degradation and remodelling that is crucial for physiological processes such as organogenesis, wound healing and angiogenesis.[42,43] Notably, MMPs are often overexpressed in tumour tissues and implicated in tumour growth, invasion and metastasis.[44,45] The development of molecular probes capable of monitoring MMP activity in live cells can advance our understanding of the roles and functions of MMPs in pathophysiological processes. Thus, we modified an MMP-2/9-cleavable peptide sequence, VPMS↓MRGG (↓ indicates the cleavage site), with a Cys residue at the N-terminus and a lysine residue at the C-terminus for the conjugation with a luminescent iridium(III) complex and an emission quencher QSY-7, respectively. The peptide CVPMSMRGGK was first reacted with complex **2** *via* the CBT–NCys condensation reaction. The resultant conjugate **2-MMP** was purified (Fig. S6 and S7, ESI†) and reacted with the *N*-hydroxysuccinimide (NHS) ester of QSY-7 to afford conjugate **2-MMP-QSY7** as a phosphorogenic substrate for MMP-2/9 (Fig. 3a). The conjugate was purified by RP-HPLC and characterised by ESI-MS (Fig. S6 and S7, ESI†). Remarkably, conjugate **2-MMP-QSY7** displayed a substantially lower emission quantum yield in degassed buffer solutions (Φ_{em} < 0.005; Table S3, ESI†) than its QSY-7-free counterpart **2-MMP** (Φ_{em} = 0.07; Table S3, ESI†). The significant emission quenching is attributed to efficient Förster resonance energy transfer (FRET) from complex **2** (λ_{em} = 580 nm) to QSY-7 (λ_{abs} = 520–600 nm) (Fig. S8, ESI†).[33,36] Analysis on the FRET parameters revealed a Förster distance (R_0) of 40.0 Å and high quenching efficiency (E_{calc}) of 0.99, which is close to the experimentally determined value (E_{expt} = 0.93) (Table S4, ESI†). The $^1O_2$ generation efficiency of conjugate **2-MMP-QSY7** (Φ_Δ = 0.06; Table S2, ESI†) was also lower than that of conjugate **2-MMP** (Φ_Δ = 0.52; Table S2, ESI†) due to efficient quenching by the appended QSY-7 moiety. Notably, upon incubation of conjugate **2-MMP-QSY7** (5 μM) with MMP-2 (0.002 mg mL^{-1}) in an aerated MMP reaction buffer for 12 h, the solution exhibited substantial emission enhancement (I/I_o = 9.8; Fig. 3b) due to enzymatic cleavage of the peptide sequence that separates the quenching QSY-7 moiety from the iridium(III) polypyridine unit, which was validated by RP-HPLC and ESI-MS analysis (Fig. S9, ESI†).

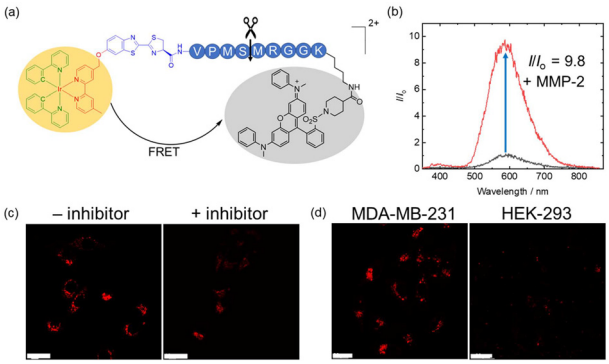

Fig. 3 (a) Structure of conjugate 2-MMP-QSY7. (b) Emission spectra of conjugate 2-MMP-QSY7 (5 μM, 12 h) in the absence (black) and presence of MMP-2 (0.002 mg mL^{-1}) (red) in aerated MMP reaction buffer/DMSO (99 : 1, v/v) at 37 °C. (c) LSCM images of live MDA-MB-231 cells incubated with conjugate 2-MMP-QSY7 (7 μM, 6 h; λ_{ex} = 405 nm, λ_{em} = 550–650 nm) without (left) and with (right) pretreatment with MMP-2/9 inhibitor I (20 μM, 2 h) at 37 °C. Scale bar = 10 μm. (d) LSCM images of live MDA-MB-231 (left) and HEK-293 cells (right) incubated with conjugate 2-MMP-QSY7 (7 μM, 6 h; λ_{ex} = 405 nm, λ_{em} = 550–650 nm) at 37 °C. Scale bar = 20 μm.

We then examined the phosphorogenic response of the conjugate towards MMP-2/9 in live cells using human breast cancer (MDA-MB-231) and human embryonic kidney (HEK-293) cells as model cell lines. As revealed by laser-scanning confocal microscopy (LSCM), MDA-MB-231 cells incubated with conjugate **2-MMP-QSY7** (7 μM, 6 h) showed intense intracellular emission, which was substantially reduced in intensity when the cells were pretreated with MMP-2/9 inhibitor I (*N*-((1,1′-biphenyl)-4-ylsulfonyl)-D-phenylalanine) (20 μM, 2 h) (Fig. 3c). Notably, when HEK-293 cells were incubated with the conjugate, only negligible intracellular emission was observed (Fig. 3d) due to the lower expression levels of MMP-2/9 in normal cells.[44,45] These results indicate that the conjugate can serve as a phosphorogenic probe for MMP-2/9 and differentiate cancer and normal cells based on MMP-2/9 activity. We further studied the (photo)cytotoxicity of conjugate **2-MMP-QSY7** towards MDA-MB-231 and HEK-293 cells. The conjugate displayed low cytotoxicity towards both cell lines in the dark ($IC_{50,dark}$ > 40 μM; Table S5, ESI†). Remarkably, it exhibited higher photocytotoxicity towards cancerous MDA-MB-231 cells ($IC_{50,light}$ = 1.93 μM) than normal HEK-293 cells ($IC_{50,light}$ = 10.17 μM) (Table S5, ESI†). The selective photocytotoxicity of the conjugate towards MDA-MB-231 cells is attributed to its distinct cellular uptake between the two cell lines (MDA-MB-231: 0.38 fmol, HEK-293: 0.03 fmol; Table S6, ESI†). We argue that the elevated MMP-2/9 secretion in cancer cells[44,45] promotes the cleavage of conjugate **2-MMP-QSY7** into its cleavage product **2-CVPMS**, which has a lower formal charge (+1) and a smaller molecular size, in the

Open Access Article. Published on 28 de gener 2025. Downloaded on 13/2/2026 2:23:50.
This article is licensed under a Creative Commons Attribution-NonCommercial 3.0 Unported Licence.

ECM, resulting in more efficient cellular uptake in cancer cells over normal cells. Thus, conjugate **2-MMP-QSY7** can serve as a phosphorogenic probe and an activatable photosensitiser for cancer cells overexpressing MMP-2/9.

Preparation of enzyme-responsive hydrogels for detecting MMP-2/9 activity in 3D cell culture

Hydrogels are water-swollen networks of polymers that are highly suitable for mimicking soft tissue due to their adjustable mechanical properties, achieved through chemical and physical cross-linking.[46] They have been widely applied in cell culture and tissue engineering.[47,48] In particular, 3D hydrogel-based cell culture models can retain surrounding ECM, preserving cell–cell and cell–ECM interactions and reproducing key biochemical and mechanical features of mammalian tissues.[49] In this regard, we designed an MMP-responsive hydrogel, termed **Gel-1**, with both cell encapsulation and MMP sensing capabilities for the *in situ* detection of MMP activity in 3D cell culture models (Fig. 4a). The gel was constructed using four components: (1) a 4-arm PEG vinylsulfone ($C(PEG\text{-}VS)_4$); (2) a 4-arm PEG thiol ($C(PEG\text{-}SH)_4$); (3) an MMP-sensitive iridium(III)–peptide conjugate **2-VPMS**, which was prepared from the reaction of complex **2** with CRDVPMSMRGGDRC (VPMS); and (4) an integrin-targeting peptide containing a Cys residue, c(RGDfC) (Fig. 4a). Poly(ethylene glycol) (PEG) is the most common macromonomer for the design of hydrogels due to its inert, non-reactive and non-degradable properties.[50] The rapid thiol–ene Michael addition reaction between the two 4-arm PEG components can enable fast gelation in aqueous solutions. Additionally, the incorporation of conjugate **2-VPMS** into the hydrogel framework can impart luminescence properties and MMP sensitivity, while that of c(RGDfC) can endow the hydrogel with cell-adhesion capability to facilitate cell encapsulation. Cells expressing elevated levels of MMPs are anticipated to trigger an increased cleavage of the VPMS peptide, thereby releasing the iridium(III) complexes that will be taken up by the cells. Thus, the intracellular emission intensity can be correlated with MMP activity, enabling the detection of enzyme activity by LSCM. An MMP-insensitive hydrogel **Gel-1C** was also prepared for comparison studies using an iridium(III)–peptide conjugate **2-VMPS**, where the iridium(III) complex was conjugated to the NCys residue of a scrambled peptide CRDVMPSRMGGDRC (VMPS).

Upon the addition of $C(PEG\text{-}SH)_4$ (30 wt%, 20 μL) in PBS (pH = 7.4, 27 μL) to a mixture of $C(PEG\text{-}VS)_4$ (30 wt%, 20 μL), **2-VPMS** (4 mM, 1 μL) and c(RGDfC) (8 mM, 5 μL) in triethanolamine (TEA) buffer (pH 8.0, 27 μL), gelation occurred within 3 min, affording **Gel-1** ([Ir] = 40 μM, 12 wt% of PEG, 100 μL). The morphology and elemental composition of **Gel-1** were studied by scanning electron microscopy (SEM) and energy dispersive X-ray spectroscopy (EDS), revealing a highly porous 3D structure that is crucial for cell encapsulation (Fig. S10, ESI†). Although the iridium content in **Gel-1** was too low to be accurately determined, the hydrogel displayed intense yellow emission upon photoirradiation at 365 nm (Fig. 5a), suggesting

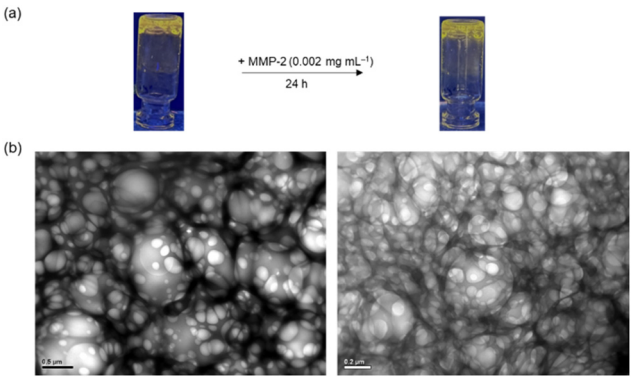

Fig. 5 (a) Photographs of **Gel-1** under UV light (λ_{ex} = 365 nm) before and after the treatment with MMP-2 (0.002 mg mL^{-1} in PBS) for 24 h. (b) TEM images of **Gel-1** before and after the treatment with MMP-2 (0.002 mg mL^{-1} in PBS) for 24 h. Scale bar = 0.5 μm (left) or 0.2 μm (right).

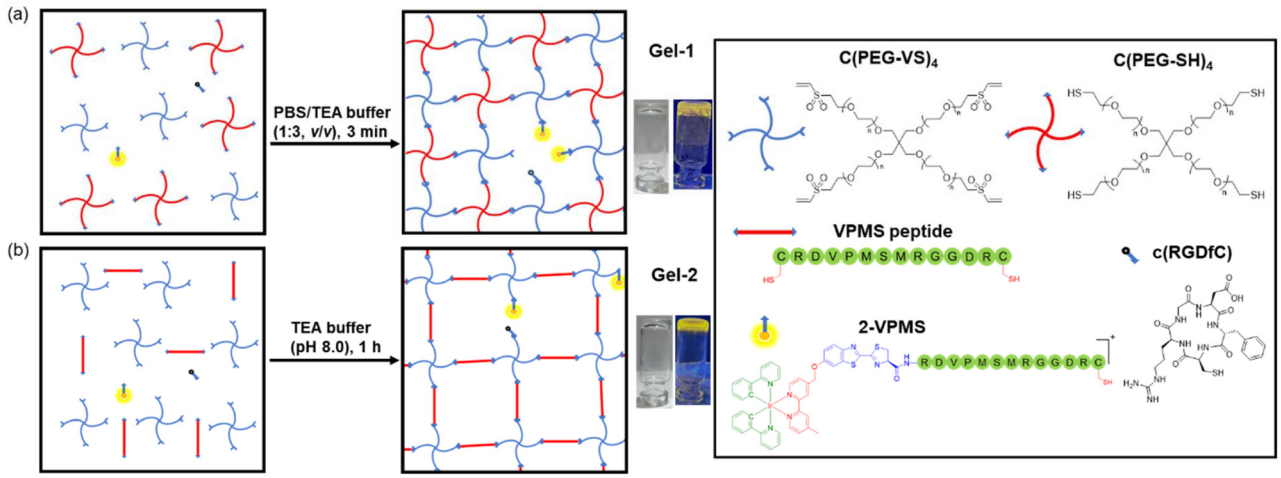

Fig. 4 Illustration of the construction of (a) **Gel-1** and (b) **Gel-2**.

This journal is © the Partner Organisations 2025

Open Access Article. Published on 28 de gener 2025. Downloaded on 13/2/2026 2:23:50.
This article is licensed under a Creative Commons Attribution-NonCommercial 3.0 Unported Licence.

the successful incorporation of the iridium(III) complex into the hydrogel structure. Notably, when the hydrogel was treated with MMP-2 (0.002 mg mL^{-1} in aerated buffer), it remained in the gel state for 24 h (Fig. 5a) due to the stable cross-links formed between the two PEG monomers. This was further confirmed by transmission electron microscopy (TEM) analysis, which showed that the porous structure of the hydrogel was largely retained after the MMP treatment (Fig. 5b). The stability of **Gel-1** in cell media was also studied, and no significant morphological changes were observed upon incubation in the dark for 72 h (Fig. S11a, ESI†).

Given the short gelation time of **Gel-1** and its high structural integrity in the presence of MMP, we then examined its application in monitoring MMP activity in 3D cell culture. An MDA-MB-231 cell suspension (*ca.* 10 000 cells) was first added to a PBS solution of $C(PEG\text{-}SH)_4$, and then mixed with a TEA buffer solution containing $C(PEG\text{-}VS)_4$, **2-VPMS** and c(RGDfC) on a confocal dish. After 10 min, a hydrogel was formed, and the cells embedded in the gel were imaged after 48 h of incubation. Under the light microscope, it was observed that the cells appeared in focus at different focal lengths, indicating that the cells were successfully encapsulated into the hydrogel to form a 3D structure (Fig. S12, ESI†). After the **Gel-1**-embedded MDA-MB-231 cells were incubated for 72 h, the viability of the cells was studied using the live/dead cell double staining assay. As revealed by LSCM, the treated cells exhibited high viability (Fig. S13, ESI†). Notably, MDA-MB-231 cells encapsulated in **Gel-1** exhibited substantially higher emission intensity than those treated with MMP-2/9 inhibitor I and those encapsulated in the MMP-insensitive hydrogel **Gel-1C** (Fig. 6a). The gradual increase in the emission intensity of MDA-MB-231 cells within **Gel-1** at different time points indicates the gradual cleavage of the VPMS peptide by MMP-2/9 and the release of the iridium(III) complex over time (Fig. S14, ESI†). The cell encapsulation capability of **Gel-1** was also tested using HEK-293 cells. While the cells were encapsulated in **Gel-1** and showed high viability (Fig. S13, ESI†), only extremely weak intracellular emission was observed (Fig. 6b), indicating minimal cleavage of the peptide due to the significantly lower expression levels of MMP-2/9 in normal cells and thus reduced release and cellular uptake of the iridium(III) complex. These results collectively demonstrate that **Gel-1** can serve as a versatile scaffold for 3D cell culture while simultaneously reporting on MMP-2/9 activity.

Preparation of enzyme-responsive hydrogels for cancer-specific imaging and photocytotoxic applications

Stimuli-responsive hydrogels can alter their network structure when exposed to external stimuli, making them ideal for applications in drug delivery, bioimaging, sensing and biomaterial fabrication.[51,52] This type of hydrogel allows for the controlled release of the encapsulated drugs at the targeted tumour site, enabling the selective induction of cytotoxicity towards tumour cells while minimising damage to surrounding normal tissues. Thus, we designed another MMP-responsive hydrogel, termed **Gel-2**, as a cancer-targeting and biodegradable carrier for the selective delivery of iridium(III) complexes to cancer cells for imaging and photocytotoxic applications. The synthetic protocol of **Gel-2** was similar to that of **Gel-1**, except that the MMP-2/9-sensitive peptide VPMS that contains a Cys residue at its two termini was used as a crosslinker instead of $C(PEG\text{-}SH)_4$ (Fig. 4b). This design can confer the hydrogel with highly controllable degradability, a feature that is crucial for regulating the release rate of the anchored iridium(III) complexes and also allows for complete clearance of the hydrogel from the body after the treatment. An MMP-insensitive hydrogel **Gel-2C** was also prepared using the scrambled peptide VMPS as the crosslinker and the corresponding conjugate **2-VMPS** for comparison studies.

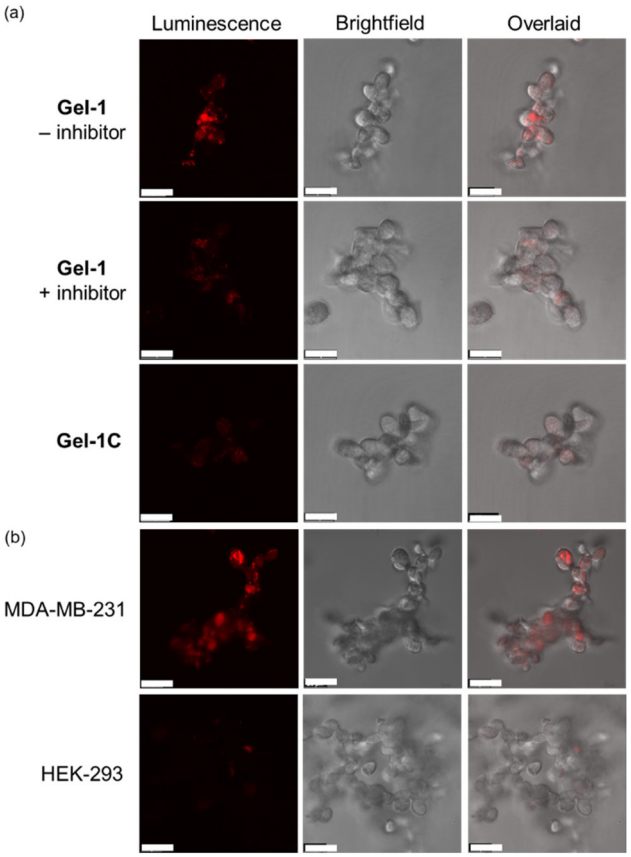

Fig. 6 (a) LSCM images of MDA-MB-231 cells encapsulated in **Gel-1** ([Ir] = 40 μM, 24 h; λ_{ex} = 405 nm, λ_{em} = 570–620 nm) without (top) and with (middle) pretreatment of MMP-2/9 inhibitor I (20 μM, 4 h), and MDA-MB-231 cells encapsulated in **Gel-1C** ([Ir] = 40 μM, 24 h; λ_{ex} = 405 nm, λ_{em} = 570–620 nm) (bottom) at 37 °C. Scale bar = 20 μm. (b) LSCM images of MDA-MB-231 (top) and HEK-293 cells (bottom) encapsulated in **Gel-1** ([Ir] = 40 μM, 24 h; λ_{ex} = 405 nm, λ_{em} = 570–620 nm) at 37 °C. Scale bar = 20 μm.

Upon the addition of the peptide VPMS (20 mM, 20 μL) to a mixture of $C(PEG\text{-}VS)_4$ (10 wt%, 25 μL), **2-VPMS** (4 mM, 2 μL) and c(RGDfC) (8 mM, 5 μL) in TEA buffer (pH 8.0, 48 μL), gelation was observed within 1 h to afford **Gel-2** ([Ir] = 80 μM, 2.5 wt% of PEG, 100 μL). As revealed by the SEM image (Fig. S15, ESI†), **Gel-2** exhibited a denser structure compared to **Gel-1** (Fig. S10, ESI†), attributed to the use of the short peptide VPMS as the crosslinker instead of the 4-arm macro-

Open Access Article. Published on 28 de gener 2025. Downloaded on 13/2/2026 2:23:50.
This article is licensed under a Creative Commons Attribution-NonCommercial 3.0 Unported Licence.

mer C(PEG-SH)$_4$. Similar to **Gel-1**, **Gel-2** showed high stability in cell culture media and remained in the gel state for up to 72 h (Fig. S11b, ESI†). However, upon treatment with MMP-2 (0.002 mg mL^{-1} in aerated buffer), it underwent complete gel–sol transition within 12 h to form a liquid solution (Fig. 7a). This is further supported by TEM analysis, showing that the hydrogel was completely degraded by MMP-2 into small scattered pieces (Fig. 7b). Similar experiments were performed using the control hydrogel **Gel-2C**, and no significant morphological changes were observed upon the MMP-2 treatment (Fig. 7c) due to the insensitivity of the scrambled peptide VMPS to MMPs.

We then examined the utilisation of **Gel-2** for the controlled delivery of the iridium(III) complexes anchored to the hydrogel framework into cancer cells based on MMP activity. We placed **Gel-2** on one side of a confocal dish seeded with MDA-MB-231 cells and allowed it to stand for 12 h (Fig. 8a). After the treatment, the hydrogel was removed and the cells were thoroughly washed with PBS prior to imaging with LSCM. Remarkably, cells located near **Gel-2** exhibited significantly higher intracellular emission intensity than the cells that were relatively distant from **Gel-2** (*ca.* 1 cm) (Fig. 8b), attributed to increased cleavage of the VPMS peptide linker in the hydrogel that led to enhanced release of the iridium(III) complex into the cells at its local surroundings. Co-staining experiments with LysoTracker Deep Red (100 nM, 30 min) confirmed the specific accumulation of the released iridium(III) complex in the lysosomes (Pearson's correlation coefficient = 0.92) after cellular uptake (Fig. 8c). However, the cells exhibited negligible intracellular emission when they were pretreated with MMP-2/9 inhibitor I (Fig. 8d), as the inhibition of MMP-2/9 activity suppressed the VPMS peptide cleavage and thereby the release of the iridium(III) complex. Similarly, cells treated with **Gel-2C** for 12 h displayed extremely weak emission even when they were located in a close proximity to the hydrogel (Fig. 8d), as the hydrogel was not degraded by the MMPs secreted from the cells. The MMP-mediated release of the iridium(III) complex from **Gel-2** was also studied in normal HEK-293 cells. Notably, while MDA-MB-231 cells showed intense punctate staining after treatment with **Gel-2**, the treated HEK-293 cells exhibited negligible intracellular emission (Fig. 8e), which is in accordance with the higher expression levels of MMPs in breast cancer cells compared to normal cells. All these results indicate that the MMP-sensitive **Gel-2** enabled the controlled release of the incorporated iridium(III) complexes into cancer cells.

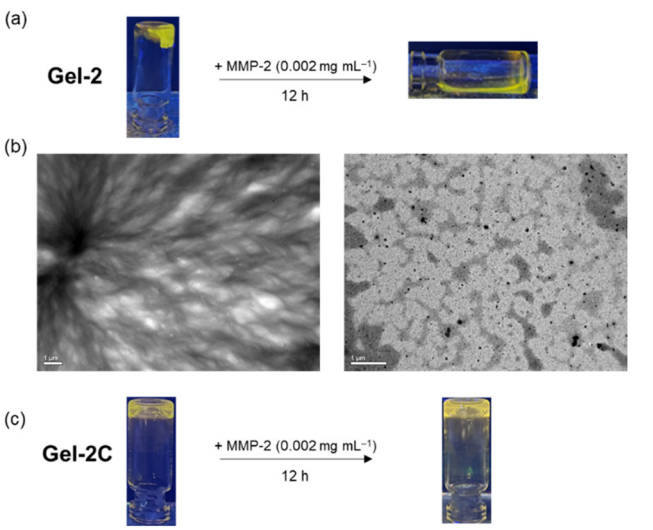

Fig. 7 (a) Photographs of **Gel-2** under UV light (λ_{ex} = 365 nm) before and after the treatment with MMP-2 (0.002 mg mL^{-1} in PBS) for 12 h. (b) TEM images of **Gel-2** before (left) and after (right) the treatment with MMP-2 (0.002 mg mL^{-1} in PBS) for 12 h. (c) Photographs of **Gel-2C** under UV light (λ_{ex} = 365 nm) before and after the treatment with MMP-2 (0.002 mg mL^{-1} in PBS) for 12 h.

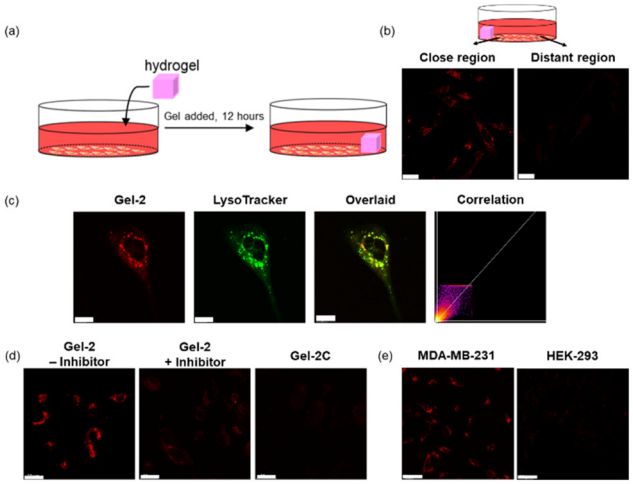

Fig. 8 (a) A schematic diagram illustrating the treatment of cells with **Gel-2**. (b) LSCM images of MDA-MB-231 cells at regions that were close to (left) and distant from (right) **Gel-2** ([Ir] = 80 μM, 12 h; λ_{ex} = 405 nm, λ_{em} = 570–620 nm). Scale bar = 20 μm. (c) LSCM images of MDA-MB-231 cells incubated with **Gel-2** ([Ir] = 80 μM, 24 h; λ_{ex} = 405 nm, λ_{em} = 570–600 nm) and LysoTracker Deep Red (100 nM, 30 min; λ_{ex} = 635 nm, λ_{em} = 650–700 nm) at 37 °C. Scale bar = 10 μm. (d) LSCM images of MDA-MB-231 cells incubated with **Gel-2** ([Ir] = 80 μM, 12 h; λ_{ex} = 405 nm, λ_{em} = 570–620 nm) without (left) and with (middle) pretreatment of MMP-2/9 inhibitor I (20 μM, 4 h), and MDA-MB-231 cells incubated with **Gel-2C** ([Ir] = 80 μM, 12 h; λ_{ex} = 405 nm, λ_{em} = 570–620 nm) (right) at 37 °C. Scale bar = 20 μm. (e) LSCM images of MDA-MB-231 (left) and HEK-293 cells (right) incubated with **Gel-2** ([Ir] = 80 μM, 12 h; λ_{ex} = 405 nm, λ_{em} = 570–620 nm). Scale bar = 20 μm. All the images in (c), (d) and (e) were taken at regions that were close to **Gel-2**.

Lysosome is an organelle that contains numerous hydrolases including cathepsins, performing cellular catabolic processes that are crucial for maintaining cell homeostasis and governing cell death.[53] Since tumour cells contain abundant lysosomes, photosensitisers that can selectively target and damage lysosomes would trigger the release of cathepsins into the cytoplasm and thereby induce cell death.[54] Given the high cancer selectivity of **Gel-2** and the strong lysosome-targeting capability of the iridium(III) complex released from the hydrogel, we examined the application of **Gel-2** in dual cancer- and lysosome-targeted photodynamic therapy (PDT). MDA-MB-231

This journal is © the Partner Organisations 2025

Open Access Article. Published on 28 de gener 2025. Downloaded on 13/2/2026 2:23:50.
This article is licensed under a Creative Commons Attribution-NonCommercial 3.0 Unported Licence.

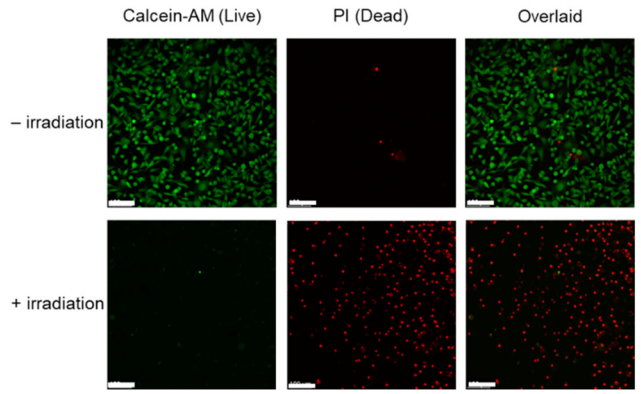

Fig. 9 Analysis of live/dead MDA-MB-231 cells using Calcein-AM (1 μM, 30 min; λ_{ex} = 488 nm, λ_{em} = 510–540 nm) and propidium iodide (PI) (3 μM, 30 min; λ_{ex} = 532 nm, λ_{em} = 610–640 nm). Top: the cells were incubated with **Gel-2** ([Ir] = 80 μM) for 24 h, then washed thoroughly with PBS, and incubated in fresh medium in the dark for 24 h. Bottom: the procedure was similar except that the cells were irradiated at 450 nm (15 mW cm^{-2}) for 30 min before the final incubation in fresh medium in the dark for 24 h. Scale bar = 100 μm. The images were taken at regions close to **Gel-2**.

cells were first treated with **Gel-2** ([Ir] = 80 μM) for 24 h, thoroughly washed with PBS, and then irradiated at 450 nm (15 mW cm^{-2}) for 30 min. After incubation for 24 h, the cell viability was examined using the live/dead cell double staining assay. As revealed by LSCM, the treated cells remained highly viable in the dark (Fig. 9, upper). However, upon irradiation, most of the cell populations were eradicated (Fig. 9, lower), which is likely due to the photogenerated ROS by the released iridium(III) complex causing damage to the lysosomes and ultimately triggered cell death. The elevated production of intracellular ROS upon irradiation of the cells was also confirmed by the chloromethyl-2′,7′-dichlorodihydrofluorescein diacetate (CM-H_2DCFDA) assay (Fig. S16, ESI†). All these results collectively indicate that the biodegradable hydrogel **Gel-2** can function as an MMP-2/9-sensitive carrier for selective delivery of luminescent iridium(III) complexes into cancer cells, and the released complexes specifically accumulated in the lysosomes and efficiently triggered cell death upon irradiation through ROS generation.

Conclusion

In summary, we developed three luminescent cyclometallated iridium(III) CBT complexes as site-specific labels for NCys. These complexes displayed high reactivity and excellent chemo- and regioselectivity towards NCys, enabling the facile preparation of photofunctional metal–peptide conjugates *via* the CBT–NCys condensation reaction. One of the CBT complexes was used to prepare an MMP-2/9-responsive metal–peptide conjugate **2-MMP-QSY7** as both a phosphorogenic probe for enzyme activity sensing in live cells and an activatable photosensitiser for cancer-targeted photocytotoxic applications. The same CBT complex was also utilised to fabricate two types of hydrogels: a non-biodegradable hydrogel **Gel-1** as a dual functional platform with both cell encapsulation and MMP-2/9 sensing capabilities for examining the enzyme activity in 3D cell culture; and a biodegradable hydrogel **Gel-2** as an MMP-2/9-sensitive carrier for selective delivery of luminescent iridium(III) complexes into cancer cells for imaging and photocytotoxic applications. We believe that the CBT complexes will serve as a new class of site-specific bioconjugation reagents with interesting photophysical properties, facilitating the construction of photofunctional peptide conjugates and biomaterials for biosensing, bioimaging, PDT and drug delivery applications.

Experimental

Materials and instruments

All solvents were of analytical reagent grade and purified according to standard procedures.[55] Triethylamine (Et_3N), Na_2CO_3, $MgSO_4$, $NaBH_4$, K_2CO_3, $AgNO_3$, KPF_6, TCEP, trifluoroacetic acid (TFA), Hdfppy, Hppy and 2-phenylquinoline-4-carboxylic acid were purchased from Acros. 6-Hydroxybenzo[*d*]thiazole-2-carbonitrile was purchased from Energy Chemical. 4,4′-Dimethyl-2,2′-bipyridine, SeO_2, $Na_2S_2O_5$ and $IrCl_3{\cdot}3H_2O$ were obtained from Aldrich. The peptides RGDPACYQGRFL, RGDPAYQGRFLC, CRGDPAYQGRFL, CVPMSMRGGK, CRDVPMSMRGGDRC (VPMS), c(RGDfC) and CRDVMPSRMGGDRC (VMPS) were purchased from GL Biochem. Polymers C(PEG-VS)$_4$ and C(PEG-SH)$_4$ were purchased from JenKem Technology USA. All these chemicals were used without further purification. 4-Carboxylaldehyde-4′-methyl-2,2′-bipyridine (bpy-CHO),[56] bpy-Br,[57] Hpqe,[58] and the iridium(III) dimers [Ir_2(N^C)$_4Cl_2$] (HN^C = Hdfppy, Hppy and Hpqe)[59] were prepared according to literature procedures. All buffer components were of biological grade and used as received. Autoclaved Milli-Q H_2O was used for the preparation of the aqueous solutions. MDA-MB-231 and HEK-293 cells were obtained from the American Type Culture Collection. QSY-7 carboxylic acid succinimidyl ester (QSY-7 NHS), human MMP-2 recombinant protein, Dulbecco's modified Eagle's medium (DMEM), fetal bovine serum (FBS), penicillin/streptomycin, PBS, trypsin-EDTA, CM-H_2DCFDA and LysoTracker Deep Red were purchased from Invitrogen. The growth medium for cell culture contained DMEM supplemented with 10% FBS and 1% penicillin/streptomycin.

^{1}H and ^{13}C NMR spectra were recorded on a Bruker 300 and 600 MHz AVANCE III spectrometer at 298 K using deuterated solvents. Chemical shifts (δ, ppm) were reported relative to tetramethylsilane (TMS). Positive-ion ESI mass spectra were recorded on a SCIEX API-3200 mass spectrometer at 298 K. Electronic absorption spectra were recorded on an Agilent 8453 diode array spectrophotometer. Steady-state emission spectra were recorded on a HORIBA Jobin Yvon FluoroMax-4 spectrofluorometer. Unless specified otherwise, all solutions for photophysical studies were degassed with no fewer than four successive freeze–pump–thaw cycles and stored in a

Open Access Article. Published on 28 de gener 2025. Downloaded on 13/2/2026 2:23:50.
This article is licensed under a Creative Commons Attribution-NonCommercial 3.0 Unported Licence.

10 cm^3 round-bottomed flask equipped with a side-arm 1 cm fluorescence cuvette and sealed from the atmosphere by a Rotaflo HP6/6 quick-release Teflon stopper. Luminescence quantum yields (Φ_{em}) were measured by the optically dilute method using an aerated aqueous solution of $[Ru(bpy)_3]Cl_2$ (Φ_{em} = 0.04, λ_{ex} = 455 nm)[60] as the standard solution. The concentrations of the standard and sample solutions were adjusted until the absorbance at 455 nm was 0.1. Emission lifetimes were measured on an Edinburgh Instruments LP920 Laser Flash Photolysis spectrometer using the third harmonic output (355 nm; 6–8 ns fwhm pulse width) of a Spectra-Physics Quanta-Ray Q-switched LAB-150 pulsed Nd:YAG laser (10 Hz) as the excitation source. HPLC was performed on an Agilent 1260 Infinity II system coupled with a diode array detector WR and 1260 Infinity II fluorescence detector using H_2O containing 0.1% (v/v) TFA (solvent A), CH_3CN containing 0.1% (v/v) TFA (solvent B) and CH_3OH containing 0.1% (v/v) TFA (solvent C) as the solvents. The diode array detector was set at 220, 350 and 560 nm.

Synthesis of bpy-CBT. To a solution of 6-hydroxybenzo[*d*]thiazole-2-carbonitrile (118 mg, 0.67 mmol) and K_2CO_3 (185 mg, 1.33 mmol) in CH_3CN (20 mL), bpy-Br (349 mg, 1.33 mmol) was added and the reaction mixture was refluxed under an inert atmosphere of nitrogen in the dark for 18 h. The brown mixture was cooled to room temperature and filtered to remove the residual solid. The resulting filtrate was purified by column chromatography on silica gel using CH_2Cl_2/EtOAc (1 : 1, v/v) as the eluent. The solvent was removed under reduced pressure to afford the product as a white solid. Yield: 204 mg (85%). ^{1}H NMR (300 MHz, $(CD_3)_2SO$, 298 K, TMS): δ 8.70 (d, J = 4.9 Hz, 1H, H6 of bpy), 8.55 (d, J = 5.0 Hz, 1H, H6′ of bpy), 8.49 (s, 1H, H3 of bpy), 8.26 (s, 1H, H3′ of bpy), 8.21 (d, J = 9.1 Hz, 1H, H5 of benzothiazole), 8.00 (s, 1H, H7 of benzothiazole), 7.54 (d, J = 4.6 Hz, 1H, H5 of bpy), 7.49 (d, J = 9.1 Hz, 1H, H4 of benzothiazole), 7.31 (d, J = 4.4 Hz, 1H, H5′ of bpy), 5.44 (s, 2H, CH_2O), 2.43 (s, 3H, CH_3 of bpy). IR (KBr) $\tilde{\nu}$/cm^{-1}: 2227 (C≡N). ESI-MS: *m*/*z* 359 $[M + H^+]^+$.

Synthesis of [Ir(dfppy)$_2$(bpy-CBT)](PF$_6$) (1). A mixture of $[Ir_2(dfppy)_4Cl_2]$ (51 mg, 0.042 mmol) and bpy-CBT (30 mg, 0.084 mmol) in CH_2Cl_2 (10 mL) was refluxed under an inert atmosphere of nitrogen in the dark for 4 h. The yellow mixture was cooled to room temperature. After addition of KPF_6 (77 mg, 0.42 mmol), the mixture was stirred at room temperature for 2 h. The solvent was removed under reduced pressure, and the yellow residual solid was purified by column chromatography on silica gel using CH_2Cl_2/CH_3OH (100 : 1, v/v) as the eluent. The solvent was removed under reduced pressure to afford a yellow solid. Subsequent recrystallisation of the solid from CH_2Cl_2/Et_2O afforded complex **1** as yellow crystals. Yield: 35 mg (78%). ^{1}H NMR (300 MHz, $(CD_3)_2CO$, 298 K, TMS): δ 9.06 (s, 1H, H3 of bpy), 8.83 (s, 1H, H3′ of bpy), 8.37 (d, J = 8.4 Hz, 2H, H6 pyridyl ring of dfppy), 8.25–8.19 (m, 2H, H4 and H7 of benzothiazole), 8.11–8.06 (m, 3H, H6 of bpy and H5 of pyridyl ring of dfppy), 7.97–7.95 (m, 3H, H6′ of bpy and H3 of pyridyl ring of dfppy), 7.89 (d, J = 4.9 Hz, 1H, H5 of bpy), 7.62 (d, J = 5.6 Hz, 1H, H5′ of bpy), 7.52 (dd, J = 9.1 and 3.0 Hz, 1H, H5 of benzothiazole), 7.30–7.24 (m, 2H, H4 of pyridyl ring of dfppy), 6.83–6.74 (m, 2H, H5 of phenyl ring of dfppy), 5.81 (m, 2H, H3 of phenyl ring of dfppy), 5.63 (s, 2H, CH_2O), 2.63 (s, 3H, CH_3 of bpy). ^{13}C NMR (150 MHz, $(CD_3)_2SO$, 298 K): δ 163.3, 158.7, 155.9, 155.0, 152.8, 150.9, 150.4, 150.0, 147.2, 140.5, 137.9, 134.9, 130.3, 128.0, 127.4, 126.5, 126.0, 124.9, 123.9, 123.4, 119.4, 113.9, 113.7, 106.4, 99.5, 68.5, 21.4. IR (KBr) $\tilde{\nu}$/cm^{-1}: 2227 (C≡N), 843 (PF_6^-). HR-ESI-MS (positive-ion mode, *m*/*z*): 931.1423 $[M - PF6^-]^+$.

Synthesis of [Ir(ppy)$_2$(bpy-CBT)](PF$_6$) (2). The synthetic procedure was similar to that for complex **1**, except that $[Ir_2(ppy)_4Cl_2]$ (150 mg, 0.14 mmol) was used instead of $[Ir_2(dfppy)_4Cl_2]$. Subsequent recrystallisation of the solid from CH_2Cl_2/Et_2O afforded complex **2** as yellow crystals. Yield: 180 mg (67%). ^{1}H NMR (300 MHz, $(CD_3)_2CO$, 298 K, TMS): δ 9.03 (s, 1H, H3 of bpy), 8.79 (s, 1H, H3′ of bpy), 8.26 (d, J = 8.1 Hz, 2H, H3 of pyridyl ring of ppy), 8.20 (d, J = 9.1 Hz, 1H, H4 of benzothiazole), 8.12 (d, J = 5.7 Hz, 1H, H6 of bpy), 8.01–7.96 (m, 4H, H7 of benzothiazole, H6′ of bpy and H3 of phenyl ring of ppy), 7.91 (d, J = 7.8 Hz, 2H, H4 of pyridyl ring of ppy), 7.87–7.85 (m, 3H, H5 of bpy and H6 of pyridyl ring of ppy), 7.58 (d, J = 4.8 Hz, 1H, H5′ of bpy), 7.52 (dd, J = 9.1 and 2.5 Hz, 1H, H5 of benzothiazole), 7.18–7.16 (m, 2H, H5 of pyridyl ring of ppy), 7.05 (t, J = 7.3 Hz, 2H, H5 of phenyl ring of ppy), 6.93 (t, J = 7.4 Hz, 2H, H6 of phenyl ring of ppy), 6.35 (q, J = 4.4 Hz, 2H, H4 of phenyl ring of ppy), 5.61 (s, 2H, CH_2O), 2.61 (s, 3H, CH_3 of bpy). ^{13}C NMR (150 MHz, $(CD_3)_2SO$, 298 K): δ 167.3, 158.7, 156.1, 155.2, 150.9, 150.3, 149.7, 149.5, 149.3, 147.1, 144.3, 139.2, 137.9, 134.9, 131.5, 130.7, 129.9, 127.1, 126.2, 126.0, 125.5, 124.3, 123.3, 122.7, 120.4, 119.4, 114.0, 106.4, 68.6, 21.3. IR (KBr) $\tilde{\nu}$/cm^{-1}: 2227 (C≡N), 843 (PF_6^-). HR-ESI-MS (positive-ion mode, *m*/*z*): 859.1797 $[M - PF_6^-]^+$.

Synthesis of [Ir(pqe)$_2$(bpy-CBT)](PF$_6$) (3). The synthetic procedure was similar to that for complex **1**, except that $[Ir_2(pqe)_4Cl_2]$ (105 mg, 0.07 mmol) was used instead of $[Ir_2(dfppy)_4Cl_2]$. Subsequent recrystallisation of the solid from CH_2Cl_2/Et_2O afforded complex **3** as red crystals. Yield: 60 mg (70%). ^{1}H NMR (300 MHz, $(CD_3)_2CO$, 298 K, TMS): δ 8.87 (s, 2H, H3 of quinolyl ring of pqe), 8.61 (s, 1H, H3 of bpy); 8.52 (d, J = 7.8 Hz, 2H, H5 of quinolyl ring of pqe), 8.38–8.32 (m, 4H, H3′ and H6 of bpy and H3 of phenyl ring of pqe), 8.21–8.15 (m, 2H, H4 and H7 of benzothiazole), 7.85 (s, 2H, H5 of benzothiazole and H6′ of bpy), 7.64–7.41 (m, 6H, H5 and H5′ of bpy and H6 and H8 of quinolyl ring of pqe), 7.26–7.06 (m, 4H, H4 of phenyl ring and H7 of quinolyl ring of pqe), 6.89 (t, J = 6.7 Hz, 2H, H5 of phenyl ring of pqe), 6.64 (d, J = 5.0 Hz, 2H, H6 of phenyl ring of pqe), 5.51 (s, 2H, CH_2O), 4.13 (s, 6H, $COOCH_3$ of pqe), 2.48 (s, 3H, CH_3 of bpy). ^{13}C NMR (150 MHz, $(CD_3)_2SO$, 298 K): δ 165.7, 158.3, 155.4, 154.5, 152.6, 151.6, 150.4, 147.1, 145.6, 139.5, 137.8, 134.5, 131.6, 129.9, 128.7, 128.5, 126.9, 125.9, 125.6, 125.6, 125.2, 125.1, 123.9, 123.5, 122.6, 119.3, 119.1, 119.0, 113.9, 106.4, 68.1, 53.8, 21.1. IR (KBr) $\tilde{\nu}$/cm^{-1}: 2227 (C≡N), 841 (PF_6^-). HR-ESI-MS (positive-ion mode, *m*/*z*): 1075.2212 $[M - PF_6^-]^+$.

This journal is © the Partner Organisations 2025

Open Access Article. Published on 28 de gener 2025. Downloaded on 13/2/2026 2:23:50.
This article is licensed under a Creative Commons Attribution-NonCommercial 3.0 Unported Licence.

Determination of $^1O_2$ generation quantum yields. The Φ_Δ values of the complexes or conjugates were evaluated by the optically dilute method[61] using $[Ru(bpy)_3]Cl_2$ in aerated CH_3CN (Φ_Δ = 0.57) as a reference.[62] An air-equilibrated CH_3CN solution (2 mL) containing the complexes or conjugates was introduced into a quartz cuvette of 1-cm path length. The concentrations of the reference and sample solutions were adjusted until the absorbance at the excitation wavelength (450 nm) was 0.15. The emission spectra of $^1O_2$ at 1200–1400 nm were recorded on an Edinburgh Instruments FLS980 spectrometer equipped with an R5509-73 NIR photomultiplier tube and C9940-02 exclusive coolers, and the Φ_Δ values of the complexes and conjugates were calculated according to the following equation, where the subscripts *s* and *r* refer to the sample and reference solutions, respectively:

$$\Phi_s = \Phi_r \left(\frac{I_r}{I_s}\right)\left(\frac{B_r}{B_s}\right)\left(\frac{n_s}{n_r}\right)^2\left(\frac{D_s}{D_r}\right)$$

where Φ is $^1O_2$ generation quantum yield, I is excitation intensity, B is $1–10^{-AL}$, A is the absorbance at the excitation wavelength, L is path length in cm, n is the refractive index of the solvent and D is integrated emission intensity.

Selectivity studies. A mixture of the iridium(III) CBT complex (150 μM), peptide (150 μM) and $NaHCO_3$ (100 μM) in PBS (pH 7.4)/CH_3CN (9 : 1, v/v, 1 mL) containing TCEP (100 μM) was stirred at 37 °C in the dark for 4 h. The reaction mixture was analysed by analytical RP-HPLC. The HPLC analyses were carried out using an Agilent analytical column (ZORBAX Eclipse Plus C18: 4.6 × 150 mm, 5 μm) with a linear gradient of 10–100% B over 25 min and a flow rate of 1 mL min^{-1}.

Preparation of iridium(III)–peptide conjugates. A mixture of complex **2** (3 μmol), the peptides CVPMSMRGGK, VPMS, or VMPS (2.8 μmol) and $NaHCO_3$ (3 μmol) in PBS (pH 7.4)/CH_3CN (9 : 1, v/v, 1 mL) containing TCEP (3 μmol) was stirred at 37 °C in the dark for 4 h. The resulting mixture was purified by RP-HPLC. The HPLC purification was performed on an Agilent semi-preparative column (ZORBAX Eclipse XDB-C18 column: 9.4 × 250 mm, 5 μm) using solvent A and solvent B with a linear gradient of 30–100% B over 30 min and a flow rate of 2 mL min^{-1}. The fractions containing the product were combined and lyophilised. The purified product was characterised by analytical RP-HPLC and ESI-MS. The HPLC analyses were carried out using an Agilent analytical column (ZORBAX Eclipse Plus C18: 4.6 × 150 mm, 5 μm) with a linear gradient of 10–100% B over 25 min and a flow rate of 1 mL min^{-1}. **2-MMP**. Yield: 5.4 mg (90%). t_R = 25.1 min. ESI-MS: *m*/*z* 637 $[M + 2 \times H^+ - CF_3CO_2^-]^{3+}$, 955 $[M + H^+ - CF_3CO_2^-]^{2+}$. **2-VPMS**. Yield: 6.7 mg (88%). t_R = 13.2 min. ESI-MS: *m*/*z* 808 $[M + 2 \times H^+ - CF_3CO_2^-]^{3+}$, 1212 $[M + H^+ - CF_3CO_2^-]^{2+}$. **2-VMPS**. Yield: 6.2 mg (81%). t_R = 13.2 min. ESI-MS: *m*/*z* 808 $[M + 2 \times H^+ - CF_3CO_2^-]^{3+}$, 1212 $[M + H^+ - CF_3CO_2^-]^{2+}$.

For conjugate **2-MMP-QSY7**, a mixture of the purified conjugate **2-MMP** (1 μmol), QSY7-NHS (1 μmol) and Et_3N (1.1 μmol) in DMF (1 mL) was stirred at 37 °C under an inert atmosphere of nitrogen in the dark for 18 h. The solvent was removed under reduced pressure, and the residual solid was purified by RP-HPLC. **2-MMP-QSY7**. Yield: 1.3 mg (50%). t_R = 18.6 min. ESI-MS: *m*/*z* 849 $[M + H^+ - CF_3CO_2^-]^{3+}$.

Förster distance measurements. The Förster distance (R_0) between the iridium(III) donor (*D*) and the QSY-7 acceptor (*A*) was calculated according to the following equation:

$$R_0(\text{in Å}) = 0.211 \times (\kappa^2 \times n^{-4} \times \Phi_D \times (\lambda))^{\frac{1}{6}}$$

where κ^2 is a factor describing the relative orientation in space of the transition dipoles of the *D* and the *A* and is assumed to be 2/3; *n* is the refractive index of the solvent; Φ_D is the emission quantum yield of conjugate **2-MMP**; $J(\lambda)$ is the overlap integral of the donor **2-MMP** emission and the acceptor QSY-7 absorption spectra.

Calculation of $J(\lambda)$ was based on the equation below:

$$J(\lambda) = \int_0^\infty F_D(\lambda) \times \varepsilon_A(\lambda) \times \lambda^4 d\lambda$$

where F_D is the corrected emission intensity of donor **2-MMP** with the emission intensity normalised to unity and ε_A is the absorption coefficient of acceptor QSY-7.

Calculated energy transfer efficiency (E_{calc}) based on Förster's theory was determined according to the following equation:

$$E_{calc} = \frac{{R_0}^6}{{R_0}^6 + r^6}$$

where *r* is the distance between the iridium(III) metal centre and the QSY-7 moiety, which was estimated by the three-dimensional structures of conjugate **2-MMP-QSY7** modulated by Chem3D 16.0.

Experimentally determined energy transfer efficiency (E_{expt}) was determined on the basis of the emission quantum yields of conjugates **2-MMP** and **2-MMP-QSY7** according to the following equation:

$$E_{expt} = 1 - \left(\frac{\Phi_{em,2\text{-MMP-QSY7}}}{\Phi_{em,2\text{-MMP}}}\right)$$

MMP-2/9 sensing by conjugate 2-MMP-QSY7. MDA-MB-231 cells in growth medium were seeded on a sterilised coverslip in a 35-mm tissue culture dish and grown at 37 °C under a 5% CO_2 atmosphere for 48 h. The medium was replaced with medium/DMSO (99 : 1, v/v) containing conjugate **2-MMP-QSY7** (7 μM). After incubation for 6 h, the cells were washed with PBS (1 mL × 3) and imaging was performed using a Leica TCS SPE (inverted configuration) confocal microscope and a 63× oil-immersion objective lens. In the negative control experiments, MDA-MB-231 cells were pretreated with MMP-2/9 inhibitor I (20 μM) for 2 h prior to incubation with conjugate **2-MMP-QSY7** or HEK-293 cells was used as the control cell line. The excitation wavelength of conjugate **2-MMP-QSY7** was 405 nm.

Photocytotoxicity assays. MDA-MB-231 or HEK-293 cells were seeded in two 96-well flat-bottomed microplates (*ca.* 10 000 cells per well) in growth medium (100 μL) and incubated at 37 °C under a 5% CO_2 atmosphere for 48 h. The

Open Access Article. Published on 28 de gener 2025. Downloaded on 13/2/2026 2:23:50.
This article is licensed under a Creative Commons Attribution-NonCommercial 3.0 Unported Licence.

growth medium was replaced with conjugate **2-MMP-QSY7** with concentrations ranging from 1 to 300 μM in medium/DMSO (99 : 1, v/v) at 37 °C under a 5% CO_2 atmosphere for 4 h. Wells containing untreated cells were used as blank control. After the treatment, the medium was removed, the cells were washed with PBS (100 μL), and phenol red-free growth medium was added to each wall (100 μL). One of the microplates was irradiated at 450 nm (15 mW cm^{-2}) for 10 min in a LED cellular photocytotoxicity irradiator (PURI Materials, Shenzhen, China), and the other microplate was kept in the dark. The culture medium was then replaced with fresh medium, and the cells were incubated at 37 °C under a 5% CO_2 atmosphere. After incubation for 24 h, the medium in each well was replaced with fresh medium (90 μL), and 10 μL of MTT (5 mg mL^{-1}) in PBS was added. The medium was removed after incubation at 37 °C for 4 h, and DMSO (100 μL) was added to each well. The microplates were further incubated at 37 °C for 20 min. The absorbance of the solutions at 570 nm was measured with BioTek Powerwave XS MQX200R microplate spectrophotometer.

Cellular uptake. MDA-MB-231 or HEK-293 cells were seeded in a 60-mm tissue culture dish and grown at 37 °C under a 5% CO_2 atmosphere for 48 h. The medium was replaced with medium/DMSO (99 : 1, v/v) containing conjugate **2-MMP-QSY7** (10 μM) at 37 °C under a 5% CO_2 atmosphere. After incubation for 3 h, the medium was removed, and the cells were washed thoroughly with PBS (1 mL × 3). The cells were trypsinised by trypsin-EDTA (500 μL) and harvested with PBS (1 mL × 3). The harvested cells, together with the collected PBS, were digested with 65% HNO_3 (1 mL) at 60 °C for 24 h. The iridium concentration in the solution was measured using a NexION 2000 ICP-MS (PerkinElmer SCIEX Instruments).

Preparation of Gel-1 and Gel-1C. To prepare **Gel-1**, a solution of **2-VPMS** (4 mM, 1 μL), c(RGDfC) (8 mM, 5 μL) and C(PEG-VS)$_4$ (30 wt%, 20 μL) in TEA buffer (pH 8.0, 27 μL) was mixed and left for 3 h. A solution of C(PEG-SH)$_4$ (30 wt%, 20 μL) in PBS (pH 7.4, 27 μL) was then added to the mixture and the reaction mixture was allowed to react at room temperature for 30 min to form **Gel-1** ([Ir] = 40 μM, 12 wt% of PEG, 100 μL). **Gel-1** was washed with PBS (1 mL × 3) before use. The preparation of the control hydrogel **Gel-1C** was similar to that of **Gel-1**, except that conjugate **2-VMPS** was used instead of conjugate **2-VPMS**.

Preparation of Gel-2 and Gel-2C. To prepare **Gel-2**, a mixture of **2-VPMS** (4 mM, 2 μL), c(RGDfC) (8 mM, 5 μL), VPMS (20 mM, 20 μL) and C(PEG-VS)$_4$ (10 wt%, 25 μL) in TEA buffer (pH 8.0, 48 μL) was allowed to react at room temperature overnight to form **Gel-2** ([Ir] = 80 μM, 2.5 wt% of PEG, 100 μL). **Gel-2** was washed with PBS (1 mL × 3) before use. The preparation of the control hydrogel **Gel-2C** was similar to that of **Gel-2**, except that VMPS and the corresponding conjugate **2-VMPS** were used instead of VPMS and conjugate **2-VPMS**, respectively.

TEM studies. The **Gel-1** or **Gel-2** reaction mixture (1 μL) was deposited onto a carbon-coated copper grid and left overnight at room temperature to form the hydrogel. The sample grid was then placed in the 50 °C oven to dry for 6 h prior to imaging. Bright-field TEM imaging was performed on a FEI tecnai 12 BioTWIN Transmission Electron Microscope operated at an acceleration voltage of 100 kV. All the TEM images were recorded by an SIS Megaview III wide-angle CCD camera or 16-bit 2 K × 2 K FEI Eagle bottom mount camera.

SEM imaging and EDS mapping. The **Gel-1** or **Gel-2** reaction mixture (50 μL) was freeze dried after gelation. The dried sample was examined using a Quattro ESEM (Thermo Fisher Scientific, Waltham, MA).

3D Cell culture and imaging by Gel-1 and Gel-1C. Conjugate **2-VPMS** (4 mM, 1 μL), c(RGDfC) (8 mM, 5 μL) and C(PEG-VS)$_4$ (30 wt%, 20 μL) in TEA buffer (27 μL) were mixed in an Eppendorf tube and left for 3 h. A suspension of MDA-MB-231 or HEK-293 cells (5 μL, *ca.* 10 000 cells) was gently added into a PBS solution (27 μL) containing C(PEG-SH)$_4$ (30 wt%, 20 μL). Then the two mixtures were added to a confocal dish, and the mixture was gently mixed and left for 10 min to form a hydrogel ([Ir] = 40 μM). Fresh medium (2 mL) was then added, and the cells were incubated at 37 °C under a 5% CO_2 atmosphere for 48 h. The cells were then imaged using a Leica TCS SPE (inverted configuration) confocal microscope and a 63× oil-immersion objective lens. In the negative control experiments, MDA-MB-231 cells were pretreated with MMP-2/9 inhibitor I (20 μM) for 4 h prior to treatment with **Gel-1** or the control hydrogel **Gel-1C** was used instead of **Gel-1**. The excitation wavelength of **Gel-1** and **Gel-1C** was 405 nm.

Live-cell confocal imaging by Gel-2 and Gel-2C. MDA-MB-231 or HEK-293 cells in growth medium were seeded on a sterilised coverslip in a 35-mm tissue culture dish and grown at 37 °C under a 5% CO_2 atmosphere for 48 h. To prepare **Gel-2**, a mixture of **2-VPMS** (4 mM, 0.6 μL), c(RGDfC) (8 mM, 1.5 μL), VPMS (20 mM, 6 μL) and C(PEG-VS)$_4$ (10 wt%, 7.5 μL) in TEA buffer (pH 8.0, 14.4 μL) was allowed to react in an Eppendorf tube at room temperature for 1 h, affording **Gel-2** ([Ir] = 80 μM) as a transparent solid. **Gel-2** was washed with PBS (1 mL × 3) before use. After the incubation period, the growth medium was removed from the cells and the cell layer was gently washed with PBS (1 mL × 3). Then **Gel-2** was added to one side of the confocal dish. After fresh medium was added, the cells were incubated at 37 °C under a 5% CO_2 atmosphere for 12 h. After that **Gel-2** and medium were removed, and the cell layer was gently washed with PBS (1 mL × 3). The cells were then imaged using a Leica TCS SPE (inverted configuration) confocal microscope and a 63× oil-immersion objective lens. In the negative control experiments, MDA-MB-231 cells were pretreated with MMP-2/9 inhibitor I (20 μM) for 4 h prior to treatment with **Gel-2** or the control hydrogel **Gel-2C** was used instead of **Gel-2**. The excitation wavelength of **Gel-2** and **Gel-2C** was 405 nm. In the co-staining experiments, after treatment with **Gel-2**, **Gel-2** and medium were removed and the cell layer was gently washed with PBS (1 mL × 3). The cells were then incubated with LysoTracker Deep Red (100 nM) in growth medium at 37 °C under a 5% CO_2 atmosphere for 30 min. The medium was then removed and the cell was gently washed with PBS (1 mL × 3) prior to

 This journal is © the Partner Organisations 2025

Open Access Article. Published on 28 de gener 2025. Downloaded on 13/2/2026 2:23:50.
This article is licensed under a Creative Commons Attribution-NonCommercial 3.0 Unported Licence.

imaging. The excitation wavelength of LysoTracker Deep Red was 635 nm. The Pearson's correlation coefficients were determined using the programme ImageJ (version 1.4.3.67).

Live/dead cell assays of hydrogel-treated cells. After treatment with **Gel-1** or **Gel-2**, the cells were incubated in fresh medium in the dark at 37 °C under a 5% CO_2 atmosphere for 24 h. The cells were then washed with PBS (1 mL × 3) and incubated in phenol red-free growth medium (100 μL) in the dark or irradiated at 450 nm (15 mW cm^{-2}) for 30 min, followed by incubation in the dark at 37 °C under a 5% CO_2 atmosphere for another 24 h. The cells were then treated with Calcein-AM (1 μM) and propidium iodide (PI) (3 μM) for 30 min, and imaged without further washing using a Leica TCS SPE (inverted configuration) confocal microscope and a 63× oil-immersion objective lens. The excitation wavelengths of Calcein-AM and PI were 488 and 532 nm, respectively.

Detection of intracellular ROS. After treatment with **Gel-2**, the cells were incubated in phenol red-free growth medium in the dark or irradiated at 450 nm (15 mW cm^{-2}) for 30 min, followed by incubation in the dark at 37 °C under a 5% CO_2 atmosphere for 2 h. The cells were then treated with CM-H_2DCFDA (10 μM) in the dark at 37 °C under a 5% CO_2 atmosphere for 30 min. After the treatment, the cells were washed with PBS (1 mL × 3) and imaged using a Leica TCS SPE (inverted configuration) confocal microscope and a 63× oil-immersion objective lens. The excitation wavelength of CM-H_2DCFDA was 488 nm.

Data availability

We confirm that all the relevant research data is contained with the manuscript and ESI.† No databases have been used and no references to such databases are contained in the manuscript or ESI.†

Conflicts of interest

There are no conflicts to declare.

Acknowledgements

We thank the Hong Kong Research Grants Council (Project No. CityU 11301121, CityU 11317022, CityU 11309423 and C7075-21GF) and the Hong Kong Research Grants Council and National Natural Science Foundation of China (Project No. N_CityU104/21). We also thank the funding support from "Laboratory for Synthetic Chemistry and Chemical Biology" under the Health@InnoHK Programme launched by Innovation and Technology Commission, The Government of Hong Kong SAR, P. R. China. We thank Mr Michael Wai-Lun Chiang of Department of Chemistry, City University of Hong Kong, for his support with the TEM and SEM measurements. J.-W. X. acknowledges the receipt of a Postgraduate Studentship administered by City University of Hong Kong.

References

1 O. Boutureira and G. J. L. Bernardes, Advances in chemical protein modification, *Chem. Rev.*, 2015, **115**, 2174–2195.
2 S. J. Walsh, J. D. Bargh, F. M. Dannheim, A. R. Hanby, H. Seki, A. J. Counsell, X. Ou, E. Fowler, N. Ashman, Y. Takada, A. Isidro-Llobet, J. S. Parker, J. S. Carroll and D. R. Spring, Site-selective modification strategies in antibody-drug conjugates, *Chem. Soc. Rev.*, 2021, **50**, 1305–1353.
3 N. Asiimwe, M. F. Al Mazid, D. P. Murale, Y. K. Kim and J.-S. Lee, Recent advances in protein modifications techniques for the targeting N-terminal cysteine, *Pept. Sci.*, 2022, **114**, e24235.
4 H. Jiang, W. Chen, J. Wang and R. Zhang, Selective N-terminal modification of peptides and proteins: Recent progresses and applications, *Chin. Chem. Lett.*, 2022, **33**, 80–88.
5 C. B. Rosen and M. B. Francis, Targeting the N terminus for site-selective protein modification, *Nat. Chem. Biol.*, 2017, **13**, 697–705.
6 P. E. Dawson, T. W. Muir, I. Clark-Lewis and S. B. H. Kent, Synthesis of proteins by native chemical ligation, *Science*, 1994, **266**, 776–779.
7 H. Ren, F. Xiao, K. Zhan, Y.-P. Kim, H. Xie, Z. Xia and J. Rao, A biocompatible condensation reaction for the labelling of terminal cysteine residues on proteins, *Angew. Chem., Int. Ed.*, 2009, **48**, 9658–9662.
8 K. Li, W. Wang and J. Gao, Fast and stable N-terminal cysteine modification through thiazolidino boronate mediated acyl transfer, *Angew. Chem., Int. Ed.*, 2020, **59**, 14246–14250.
9 A. Bandyopadhyay, S. Cambray and J. Gao, Fast and selective labelling of N-terminal cysteines at neutral pH *via* thiazolidino boronate formation, *Chem. Sci.*, 2016, **7**, 4589–4593.
10 H. Faustino, M. J. S. A. Silva, L. F. Veiros, G. J. L. Bernardes and P. M. P. Gois, Iminoboronates are efficient intermediates for selective, rapid and reversible *N*-terminal cysteine functionalisation, *Chem. Sci.*, 2016, **7**, 5052–5058.
11 X. Zheng, Z. Li, W. Gao, X. Meng, X. Li, L. Y. P. Luk, Y. Zhao, Y.-H. Tsai and C. Wu, Condensation of 2-((alkylthio)(aryl)methylene)malononitrile with 1,2-aminothiol as a novel bioorthogonal reaction for site-specific protein modification and peptide cyclization, *J. Am. Chem. Soc.*, 2020, **142**, 5097–5103.
12 A. Istrate, M. B. Geeson, C. D. Navo, B. B. Sousa, M. C. Marques, R. J. Taylor, T. Journeaux, S. R. Oehler, M. R. Mortensen, M. J. Deery, A. D. Bond, F. Corzana, G. Jiménez-Osés and G. J. L. Bernardes, Platform for orthogonal *N*-cysteine-specific protein modification enabled by cyclopropenone reagents, *J. Am. Chem. Soc.*, 2022, **144**, 10396–10406.
13 Y. Yuan and G. Liang, A biocompatible, highly efficient click reaction and its applications, *Org. Biomol. Chem.*, 2014, **12**, 865–871.

Open Access Article. Published on 28 de gener 2025. Downloaded on 13/2/2026 2:23:50.
This article is licensed under a Creative Commons Attribution-NonCommercial 3.0 Unported Licence.

14 M. Zhang and G. Liang, Applications of CBT-Cys click reaction: Past, present, and future, *Sci. China Chem.*, 2018, **61**, 1088–1098.
15 X. Hu, R. Tang, L. Bai, S. Liu, G. Liang and X. Sun, CBT-Cys click reaction for optical bioimaging in vivo, *VIEW*, 2023, **4**, 20220065.
16 L. C.-C. Lee, L. Huang, P. K.-K. Leung and K. K.-W. Lo, Recent development of photofunctional transition metal–peptide conjugates for bioimaging and therapeutic applications, *Eur. J. Inorg. Chem.*, 2022, **2022**, e202200455.
17 K. S. Gkika, D. Cullinane and T. E. Keyes, Metal peptide conjugates in cell and tissue imaging and biosensing, *Top. Curr. Chem.*, 2022, **380**, 30.
18 L. C.-C. Lee and K. K.-W. Lo, Shining new light on biological systems: Luminescent transition metal complexes for bioimaging and biosensing applications, *Chem. Rev.*, 2024, **124**, 8825–9014.
19 X. Ma, J. Jia, R. Cao, X. Wang and H. Fei, Histidine–iridium(III) coordination-based peptide luminogenic cyclisation and cyclo-RGD peptides for cancer-cell targeting, *J. Am. Chem. Soc.*, 2014, **136**, 17734–17737.
20 K. Vellaisamy, G. Li, W. Wang, C.-H. Leung and D.-L. Ma, A long-lived peptide-conjugated iridium(III) complex as a luminescent probe and inhibitor of the cell migration mediator, formyl peptide receptor 2, *Chem. Sci.*, 2018, **9**, 8171–8177.
21 Z. Zhao, X. Zhang, C.-E. Li and T. Chen, Designing luminescent ruthenium prodrug for precise cancer therapy and rapid clinical diagnosis, *Biomaterials*, 2019, **192**, 579–589.
22 W. Wang, K.-J. Wu, K. Vellaisamy, C.-H. Leung and D.-L. Ma, Peptide-conjugated long-lived theranostic imaging for targeting GRPr in cancer and immune cells, *Angew. Chem., Int. Ed.*, 2020, **59**, 17897–17902.
23 C. A. Puckett and J. K. Barton, Fluorescein redirects a ruthenium–octaarginine conjugate to the nucleus, *J. Am. Chem. Soc.*, 2009, **131**, 8738–8739.
24 A. Byrne, C. S. Burke and T. E. Keyes, Precision targeted ruthenium(II) luminophores; highly effective probes for cell imaging by stimulated emission depletion (STED) microscopy, *Chem. Sci.*, 2016, **7**, 6551–6562.
25 S. Ji, X. Yang, X. Chen, A. Li, D. Yan, H. Xu and H. Fei, Structure-tuned membrane active Ir-complexed oligoarginine overcomes cancer cell drug resistance and triggers immune responses in mice, *Chem. Sci.*, 2020, **11**, 9126–9133.
26 A. Martin, A. Byrne, C. S. Burke, R. J. Forster and T. E. Keyes, Peptide-bridged dinuclear Ru(II) complex for mitochondrial targeted monitoring of dynamic changes to oxygen concentration and ROS generation in live mammalian cells, *J. Am. Chem. Soc.*, 2014, **136**, 15300–15309.
27 C. S. Burke, A. Byrne and T. E. Keyes, Highly selective mitochondrial targeting by a ruthenium(II) peptide conjugate: Imaging and photoinduced damage of mitochondrial DNA, *Angew. Chem., Int. Ed.*, 2018, **57**, 12420–12424.
28 C. S. Burke, A. Byrne and T. E. Keyes, Targeting photoinduced DNA destruction by Ru(II) tetraazaphenanthrene in live cells by signal peptide, *J. Am. Chem. Soc.*, 2018, **140**, 6945–6955.
29 A. H. Day, M. H. Übler, H. L. Best, E. Lloyd-Evans, R. J. Mart, I. A. Fallis, R. K. Allemann, E. A. H. Al-Wattar, N. I. Keymer, N. J. Buurma and S. J. A. Pope, Targeted cell imaging properties of a deep red luminescent iridium(III) complex conjugated with a c-Myc signal peptide, *Chem. Sci.*, 2020, **11**, 1599–1606.
30 Q. Wu, K. Y. Zhang, P. Dai, H. Zhu, Y. Wang, L. Song, L. Wang, S. Liu, Q. Zhao and W. Huang, Bioorthogonal "labelling after recognition" affording an FRET-based luminescent probe for detecting and imaging caspase-3 via photoluminescence lifetime imaging, *J. Am. Chem. Soc.*, 2020, **142**, 1057–1064.
31 C. Jin, G. Li, X. Wu, J. Liu, W. Wu, Y. Chen, T. Sasaki, H. Chao and Y. Zhang, Robust packing of a self-assembling iridium complex via endocytic trafficking for long-term lysosome tracking, *Angew. Chem., Int. Ed.*, 2021, **60**, 7597–7601.
32 L. C.-C. Lee, A. W.-Y. Tsang, H.-W. Liu and K. K.-W. Lo, Photofunctional cyclometalated iridium(III) polypyridine complexes bearing a perfluorobiphenyl moiety for bioconjugation, bioimaging, and phototherapeutic Applications, *Inorg. Chem.*, 2020, **59**, 14796–14806.
33 P. K.-K. Leung, L. C.-C. Lee, T. K.-Y. Ip, H.-W. Liu, S.-M. Yiu, N. P. Lee and K. K.-W. Lo, Luminescent rhenium(I) perfluorobiphenyl complexes as site-specific labels for peptides to afford photofunctional bioconjugates, *Chem. Commun.*, 2021, **57**, 11256–11259.
34 L. Huang, P. K.-K. Leung, L. C.-C. Lee, G.-X. Xu, Y.-W. Lam and K. K.-W. Lo, Photofunctional cyclometallated iridium(III) polypyridine methylsulfone complexes as sulfhydryl-specific reagents for bioconjugation, bioimaging and photocytotoxic applications, *Chem. Commun.*, 2022, **58**, 10162–10165.
35 J. Shum, L. C.-C. Lee, M. W.-L. Chiang, Y.-W. Lam and K. K.-W. Lo, A concerted enzymatic and bioorthogonal approach for extra- and intracellular activation of environment-sensitive ruthenium(II)-based imaging probes and photosensitizers, *Angew. Chem., Int. Ed.*, 2023, **62**, e202303931.
36 L. Huang, L. C.-C. Lee, J. Shum, G.-X. Xu and K. K.-W. Lo, Construction of photofunctional peptide conjugates through selective modification of N-terminal cysteine with cyclometallated iridium(III) 2-formylphenylboronic acid complexes for organelle-specific imaging, enzyme activity sensing and photodynamic therapy, *Chem. Commun.*, 2024, **60**, 6186–6189.
37 E. C.-L. Mak, Z. Chen, L. C.-C. Lee, P. K.-K. Leung, A. M.-H. Yip, J. Shum, S.-M. Yiu, V. W.-W. Yam and K. K.-W. Lo, Exploiting the potential of iridium(III) *bis*-nitrone complexes as phosphorogenic bifunctional reagents for phototheranostics, *J. Am. Chem. Soc.*, 2024, **146**, 25589–25599.
38 M. S. Lowry, W. R. Hudson, R. A. Pascal and S. Bernhard, Accelerated luminophore discovery through combinatorial synthesis, *J. Am. Chem. Soc.*, 2004, **126**, 14129–14135.

 This journal is © the Partner Organisations 2025

Open Access Article. Published on 28 de gener 2025. Downloaded on 13/2/2026 2:23:50.
This article is licensed under a Creative Commons Attribution-NonCommercial 3.0 Unported Licence.

39 K. Y. Zhang, H.-W. Liu, M.-C. Tang, A. W.-T. Choi, N. Zhu, X.-G. Wei, K.-C. Lau and K. K.-W. Lo, Dual-emissive cyclometalated iridium(III) polypyridine complexes as ratiometric biological probes and organelle-selective bioimaging reagents, *Inorg. Chem.*, 2015, **54**, 6582–6593.
40 K. P. S. Zanoni, A. Ito, M. Grüner, N. Y. Murakami Iha and A. S. S. de Camargo, Photophysical dynamics of the efficient emission and photosensitization of $[Ir(pqi)_2(NN)]^+$ complexes, *Dalton Trans.*, 2018, **47**, 1179–1188.
41 S. Ahmed, A. S. Mathews, N. Byeon, A. Lavasanifar and K. Kaur, Peptide arrays for screening cancer specific peptides, *Anal. Chem.*, 2010, **82**, 7533–7541.
42 A. Jabłońska-Trypuć, M. Matejczyk and S. Rosochacki, Matrix metalloproteinases (MMPs), the main extracellular matrix (ECM) enzymes in collagen degradation, as a target for anticancer drugs, *J. Enzyme Inhib. Med. Chem.*, 2016, **31**, 177–183.
43 A. Page-McCaw, A. J. Ewald and Z. Werb, Matrix metalloproteinases and the regulation of tissue remodelling, *Nat. Rev. Mol. Cell Biol.*, 2007, **8**, 221–233.
44 R. Roy, J. Yang and M. A. Moses, Matrix metalloproteinases as novel biomarkers and potential therapeutic targets in human cancer, *J. Clin. Oncol.*, 2009, **27**, 5287–5297.
45 M. Egeblad and Z. Werb, New functions for the matrix metalloproteinases in cancer progression, *Nat. Rev. Cancer*, 2002, **2**, 161–174.
46 S. A. Fisher, A. E. G. Baker and M. S. Shoichet, Designing peptide and protein modified hydrogels: Selecting the optimal conjugation strategy, *J. Am. Chem. Soc.*, 2017, **139**, 7416–7427.
47 S. R. Caliari and J. A. Burdick, A practical guide to hydrogels for cell culture, *Nat. Methods*, 2016, **13**, 405–414.
48 V. Nele, J. P. Wojciechowski, J. P. K. Armstrong and M. M. Stevens, Tailoring gelation mechanisms for advanced hydrogel applications, *Adv. Funct. Mater.*, 2020, **30**, 2002759.
49 C. Jensen and Y. Teng, Is it time to start transitioning from 2D to 3D cell culture?, *Front. Mol. Biosci.*, 2020, **7**, 513823.
50 T. R. Hoare and D. S. Kohane, Hydrogels in drug delivery: Progress and challenges, *Polymer*, 2008, **49**, 1993–2007.
51 X. Ma, K. P. C. Sekhar, P. Zhang and J. Cui, Advances in stimuli-responsive injectable hydrogels for biomedical applications, *Biomater. Sci.*, 2024, **12**, 5468–5480.
52 H. Zhou, Y. Zhu, B. Yang, Y. Huo, Y. Yin, X. Jiang and W. Ji, Stimuli-responsive peptide hydrogels for biomedical applications, *J. Mater. Chem. B*, 2024, **12**, 1748–1774.
53 L. Schneider and J. Zhang, Lysosomal function in macromolecular homeostasis and bioenergetics in Parkinson's disease, *Mol. Neurodegener.*, 2010, **5**, 14.
54 M. Ghosh, F. Carlsson, A. Laskar, X.-M. Yuan and W. Li, Lysosomal membrane permeabilization causes oxidative stress and ferritin induction in macrophages, *FEBS Lett.*, 2011, **585**, 623–629.
55 W. L. F. Armarego and C. Chai, *Purification of laboratory chemicals*, 6th edn, Butterworth-Heinemann, Oxford, 2009.
56 B. M. Peek, G. T. Ross, S. W. Edwards, G. J. Meyer, T. J. Meyer and B. W. Erickson, Synthesis of redox derivatives of lysine and related peptides containing phenothiazine or tris(2,2′-bipyridine)ruthenium(II), *Int. J. Pept. Protein Res.*, 1991, **38**, 114–123.
57 B. D. Sherman, Y. Xie, M. V. Sheridan, D. Wang, D. W. Shaffer, T. J. Meyer and J. J. Concepcion, Light-driven water splitting by a covalently linked ruthenium-based chromophore–catalyst assembly, *ACS Energy Lett.*, 2017, **2**, 124–128.
58 T. S.-M. Tang, K.-K. Leung, M.-W. Louie, H.-W. Liu, S. H. Cheng and K. K.-W. Lo, Phosphorescent biscyclometallated iridium(III) ethylenediamine complexes functionalised with polar ester or carboxylate groups as bioimaging and visualisation reagents, *Dalton Trans.*, 2015, **44**, 4945–4956.
59 M. Nonoyama, Benzo[*h*]quinolin-10-yl-*N* iridium(III) complexes, *Bull. Chem. Soc. Jpn.*, 1974, **47**, 767–768.
60 K. Suzuki, A. Kobayashi, S. Kaneko, K. Takehira, T. Yoshihara, H. Ishida, Y. Shiina, S. Oishi and S. Tobita, Reevaluation of absolute luminescence quantum yields of standard solutions using a spectrometer with an integrating sphere and a back-thinned CCD detector, *Phys. Chem. Chem. Phys.*, 2009, **11**, 9850–9860.
61 J. N. Demas and G. A. Crosby, Measurement of photoluminescence quantum yields. Review, *J. Phys. Chem.*, 1971, **75**, 991–1024.
62 A. A. Abdel-Shafi, P. D. Beer, R. J. Mortimer and F. Wilkinson, Photosensitised generation of singlet oxygen from ruthenium(II)-substituted benzoaza-crown-bipyridine complexes, *Phys. Chem. Chem. Phys.*, 2000, **2**, 3137–3144.